Geophys. J. Int. (2009) **179,** 112–124 doi: 10.1111/j.1365-246X.2009.04297.x

Using analytic signal to determine magnetization/density ratios of geological structures

Wen-Bin Doo, Shu-Kun Hsu, Ching-Hui Tsai and Yin-Sheng Huang

Institute of Geophysics, National Central University, Taiwan. E-mail: wenbindoo@gmail.com

Accepted 2009 June 12. Received 2009 June 11; in original form 2008 November 12

SUMMARY

The Poisson theorem provides a simple relationship between the gravity and magnetic potentials, which is useful in interpreting joint data sets of gravity and magnetic data. Based on the simple Poisson theorem, magnetization/density ratio (MDR) can be estimated. However, potential field data is often ambiguous in datum level and multisources interference that may cause bias in interpretation. Here, we propose an improved Poisson theorem to estimate MDR by using analytic signals of gravity and magnetic data. The major advantage of using the analytic signal is that we can also determine the sources locations and boundaries supposing that we know the ambient magnetic parameters. Besides, we can also avoid the determination error from uncertain datum levels.

We demonstrate the feasibility of the proposed method in 2-D and 3-D synthetic models. The proposed method is also applied to a profile across the offshore area of northern Taiwan. Comparing with the reflection seismic profile, our result can help identify the existence of a deep-seated igneous body beneath the area of Mienhuayu and Pengchiagu islands off northern Taiwan.

Key words: Magnetic anomalies: modelling and interpretation; Rock and mineral magnetism; Marine magnetics and palaeomagnetics.

1 INTRODUCTION

Gravity and magnetic data are often processed and interpreted separately. Using a suitable theoretical background, we can put the interpretation of gravity and magnetic anomalies together. The mathematical relationship between magnetic and gravity data, was described by the Poisson relation (Garland 1951; Grant & West 1965). To valid this, an isolated source must have a uniform density and magnetization contrast. The relationship, however, is independent of the shape and location of the source. Therefore, the magnetic field can be calculated directly from the gravity field without knowing the geometry of the body or how magnetization and density are distributed within the body.

There are several methods of application of Poisson theorem that have declared to be useful in the combined analysis of gravity and magnetic data. For example, the theorem has been used to determine the magnetization/density ratios (MDRs) (Garland 1951; Chandler *et al.* 1981; Hildebrand 1985; Chandler & Malek 1991; Mendonca 2004) and magnetization direction (Ross & Lavin 1966; Cordell & Taylor 1971; Mendonca 2004). Wilson (1970) demonstrated that this theorem can be used to separate interfering anomalies if the physical properties of the source were known. A drawback of using simple Poisson theorem is the datum levels of gravity or magnetic data are usually uncertain.

In this study we propose to combine a 3-D analytic signal method and Poisson theorem to calculate the MDR value. The amplitude of the simple analytic signal is defined as the square root of the squared sum of the vertical and two horizontal derivatives of the magnetic field (Roest *et al.* 1992). The outlines of the geological boundaries can be determined by tracing the maximum amplitudes of the analytic signal. The analytic signal exhibits maximum amplitudes over magnetization contrasts. Hence, the advantage is that in addition to the geological boundaries indicated by the maximum amplitudes of analytic signals, we can determine the MDR without considering the datum levels.

2 METHODOLOGY

For a point outside the source of an arbitrary shape, the magnetic potential U_m and gravity potential U_g are linked by the Poisson theorem (Poisson 1826)

$$U_m = \frac{1}{G}\frac{\Delta M}{\Delta \rho}\frac{\partial U_g}{\partial m} \tag{1}$$

where G is the universal gravitational constant, $\Delta\rho$ is the density contrast at the point within the source and ΔM is the magnetization contrast at the same position, m is the direction of source magnetization. Based on the Poisson theorem, the spatial distribution of the MDR (i.e. $\Delta M/\Delta\rho$) can be calculated which provides an effective way of discriminating rock type. However, one problem is that we generally observe potential fields instead of potentials.

Applying the 3-D gradient operator $\nabla = \frac{\partial}{\partial x}\hat{i} + \frac{\partial}{\partial y}\hat{j} + \frac{\partial}{\partial z}\hat{k}$ on both sides of eq. (1), the vector magnetic field $\vec{T}_m$ is then acquired

$$\vec{T}_m = \frac{\partial U_m}{\partial x}\hat{i} + \frac{\partial U_m}{\partial y}\hat{j} + \frac{\partial U_m}{\partial z}\hat{k} = \frac{1}{G}\frac{\Delta M}{\Delta \rho}\nabla\frac{\partial U_g}{\partial m}. \quad (2)$$

Assuming vertical magnetization, Mendonca (2004) obtained

$$\vec{T}_z = \frac{1}{G}\frac{\Delta M}{\Delta \rho}\nabla g_z.$$

In that case,

$$\left|\vec{T}_m\right| = \left|\vec{T}_z\right| \text{ and } MDR = G\frac{\left|\vec{T}_m\right|}{|\nabla \cdot g_z|}. \quad (3)$$

A general analytic signal is defined in Hsu *et al.* (1996) as

$$A_n(x, y) = \frac{\partial}{\partial x}\left(\frac{\partial^n F}{\partial z^n}\right)\hat{i} + \frac{\partial}{\partial y}\left(\frac{\partial^n F}{\partial z^n}\right)\hat{j} + \frac{\partial}{\partial z}\left(\frac{\partial^n F}{\partial z^n}\right)\hat{k},$$

where F is the potential field anomaly and the amplitude of nth-order analytic signal $|A_n(x, y)| = \sqrt{\left(\frac{\partial}{\partial x}\frac{\partial^n F}{\partial z^n}\right)^2 + \left(\frac{\partial}{\partial y}\frac{\partial^n F}{\partial z^n}\right)^2 + \left(\frac{\partial}{\partial z}\frac{\partial^n F}{\partial z^n}\right)^2}$.

By vertically deriving eq. (3),

$$\text{MDR} = G\frac{\left|\vec{T}_m\right|}{|\nabla \cdot g_z|} = G\frac{\frac{\partial}{\partial z}\left|\vec{T}_m\right|}{\frac{\partial}{\partial z}|\nabla \cdot g_z|} = G\frac{\left|\frac{\partial \vec{T}_m}{\partial z}\right|}{\left|\nabla \cdot \frac{\partial g_z}{\partial z}\right|}. \quad (4)$$

$\left|\frac{\partial \vec{T}_m}{\partial z}\right| = \sqrt{\left(\frac{\partial}{\partial x}\frac{\partial U_m}{\partial z}\right)^2 + \left(\frac{\partial}{\partial y}\frac{\partial U_m}{\partial z}\right)^2 + \left(\frac{\partial}{\partial z}\frac{\partial U_m}{\partial z}\right)^2}$ is the amplitude of the simple analytic signal of magnetic data, and $\left|\nabla \cdot \frac{\partial g_z}{\partial z}\right| = \sqrt{\left(\frac{\partial}{\partial x}\frac{\partial g_z}{\partial z}\right)^2 + \left(\frac{\partial}{\partial y}\frac{\partial g_z}{\partial z}\right)^2 + \left(\frac{\partial}{\partial z}\frac{\partial g_z}{\partial z}\right)^2}$ is the first-order analytic signal of the gravity data. Thus,

$$\text{MDR} = G\frac{|MAS_0|}{|GAS_1|}, \quad (5)$$

where $|MAS_0|$ represents the amplitude of simple zeroth-order analytic signal of magnetic anomaly and $|GAS_1|$ represents the amplitude of first-order analytic signal of gravity anomaly.

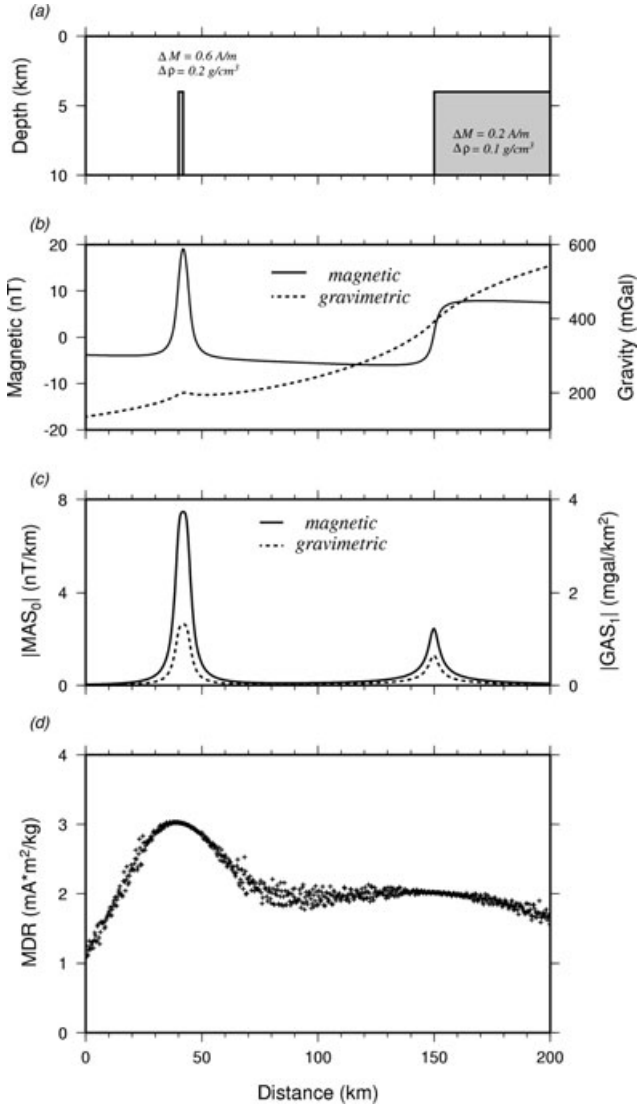

Figure 1. 1-D model test. (a) Model geometry, (b) magnetic and gravity anomalies caused by subsurface sources, (c) amplitude of the gravity first-order analytic signal ($|GAS_1|$) and amplitude of the magnetic zero-order analytic signal ($|MAS_0|$) and (d) MDR values distribution.

3 SYNTHETIC MODELS

In order to demonstrate the feasibility of the proposed method, we use one 2-D model and three 3-D models for testing. The parameters of models are shown in Table 1.

3.1 2-D model

First, we use a 2-D model, which contains a thin dyke and a contact (Fig. 1). The density and magnetization contrast of the sources are set as 0.2 g cm^{-3} and 0.6 A m^{-1} for the thin dyke and 0.1 g cm^{-3}

Table 1. Magnetic parameters of the test models.

Model		Length along X-axis (km)	Length along Y-axis (km)	H1 (km)	H2 (km)	$\Delta\rho$	ΔM	Theoretical MDR (10^{-3}Am^2 kg^{-1})	Estimated MDR (10^{-3}Am^2 kg^{-1})
Model 1 (see Fig. 1)	Dyke	1	–	4	24	0.2	0.6	3.0	3.02
	Contact	Infinite	–	4	24	0.1	0.2	2.0	2.02
Model 2 (see Fig. 2)	Prism	100	100	2	12	0.4	1.2	3.0	3.01
Model 3 (see Fig. 3)	Prism	2	2	4	14	0.4	0.4	1.0	0.92
Model 4 (see Fig. 4)	Prism 4A	50	50	2	22	0.4	1.2	3.0	2.78
	Prism 4B	80	200	2	22	0.2	0.3	1.5	1.31

Note: H1 is depth to the top surface of each model, H2 is depth to the bottom of the model, $\Delta\rho$ is density contrast (g cm^{-3}) and ΔM is magnetization contrast (A m^{-1}).

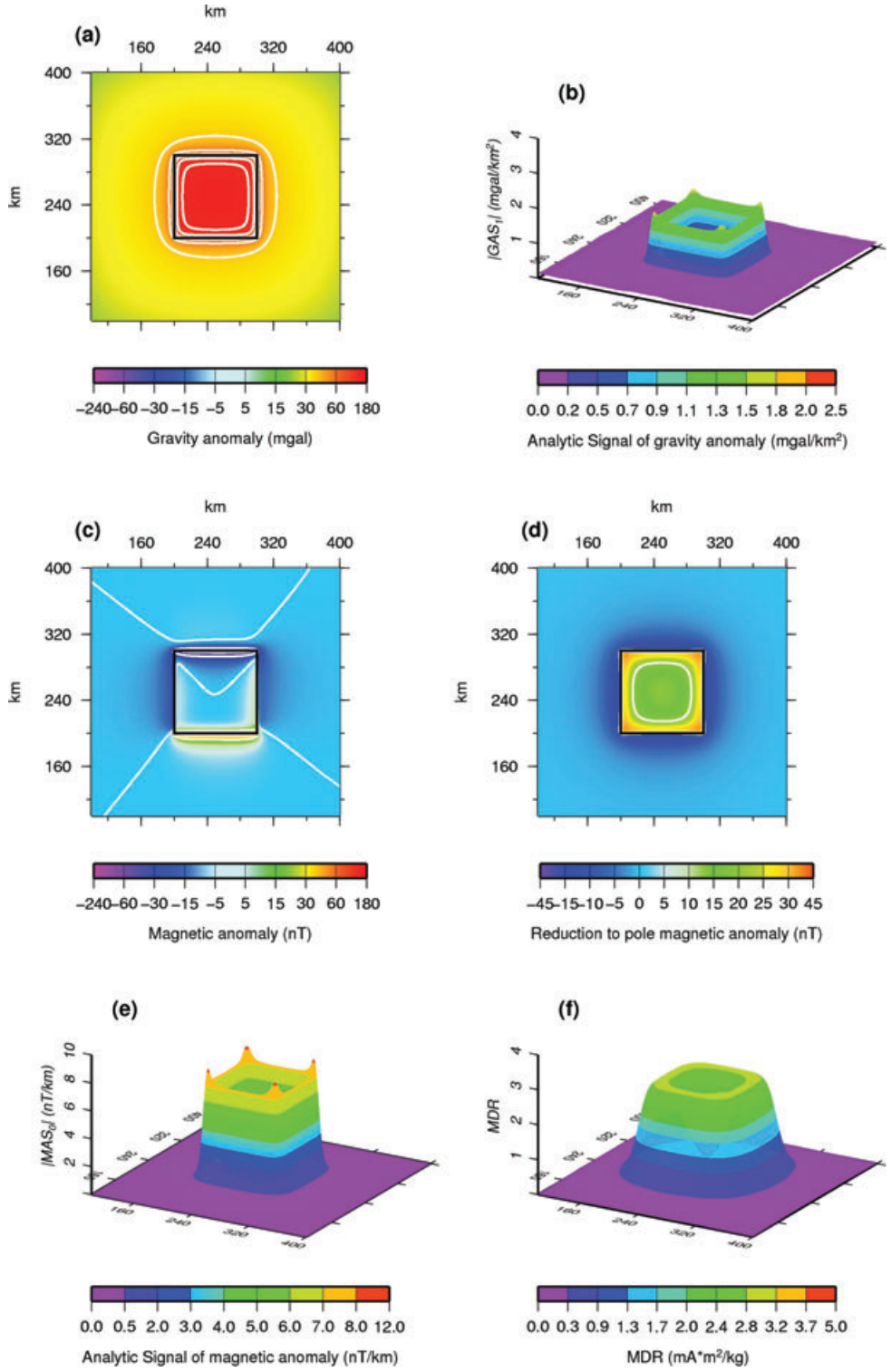

Figure 2. (a) Gravity anomaly, thick block indicate the source boundary, (b) amplitude of the gravity first-order analytic signal, (c) magnetic anomaly, thick block indicate the source boundary, (d) reduction to pole magnetic anomaly, (e) amplitude of the magnetic zero-order analytic signal and (f) MDR values distribution.

and 0.2 A m^{-1} for the contact (Fig. 1). Inclination and declination of these two sources are set as 90° and 0° (vertical magnetization). In the result of the 2-D model test, we can find the correct MDR values focus at the peaks of the analytic signals (*cf*. Figs 1c and d).

3.2 3-D models

The 3-D model shown in Fig. 2 is an isolated source. Magnetization inclination and declination of 3-D models are set as 35° and −5°, respectively. In Fig. 2, the source is a square prism of

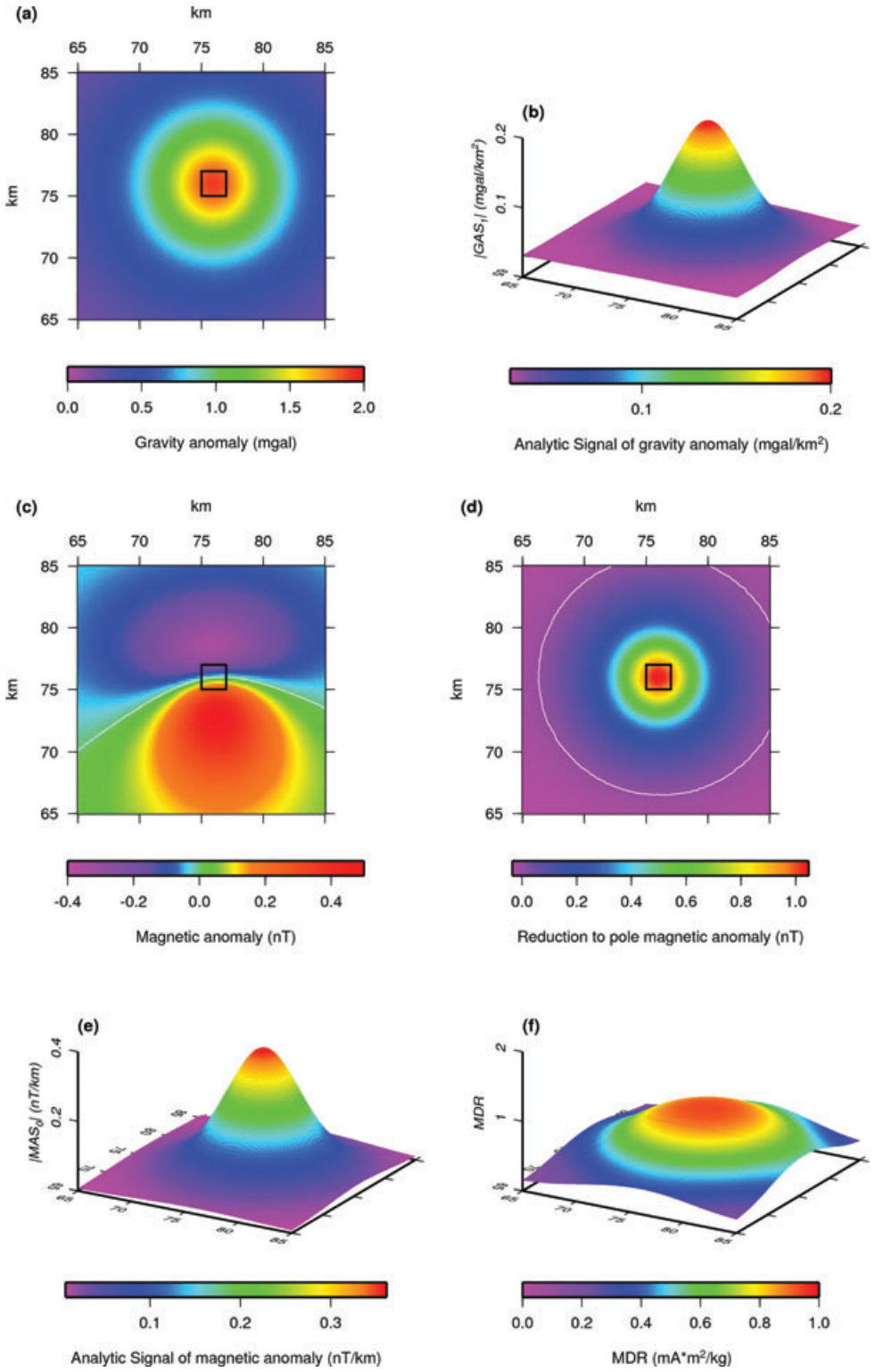

Figure 3. (a) Gravity anomaly, thick block indicate the source boundary, (b) amplitude of the gravity first-order analytic signal, (c) magnetic anomaly, thick block indicate the source boundary, (d) reduction to pole magnetic anomaly, (e) amplitude of the magnetic zero-order analytic signal and (f) MDR values distribution.

100 km × 100 km × 10 km. The distance to the top of the prism is 2 km between the seafloor. The background density and magnetization are 2.4 g cm^{-3} and 0.02 A m^{-1} and the density and magnetization of the square prism are in 2.8 g cm^{-3} and 1.22 A m^{-1}. The gravity anomaly is shown in Fig. 2(a) and the magnetic anomaly is shown in Fig. 2(c). The reduced to the pole magnetic anomaly is shown in Fig. 2(d). We use 0.5 km × 0.5 km grid to calculate simple zeroth-order analytic signal of magnetic data and its amplitude (Fig. 2e). The amplitude of the first-order analytic signal of gravity data is shown in Fig. 2(b). From Figs 2(e) and (b), we can estimate

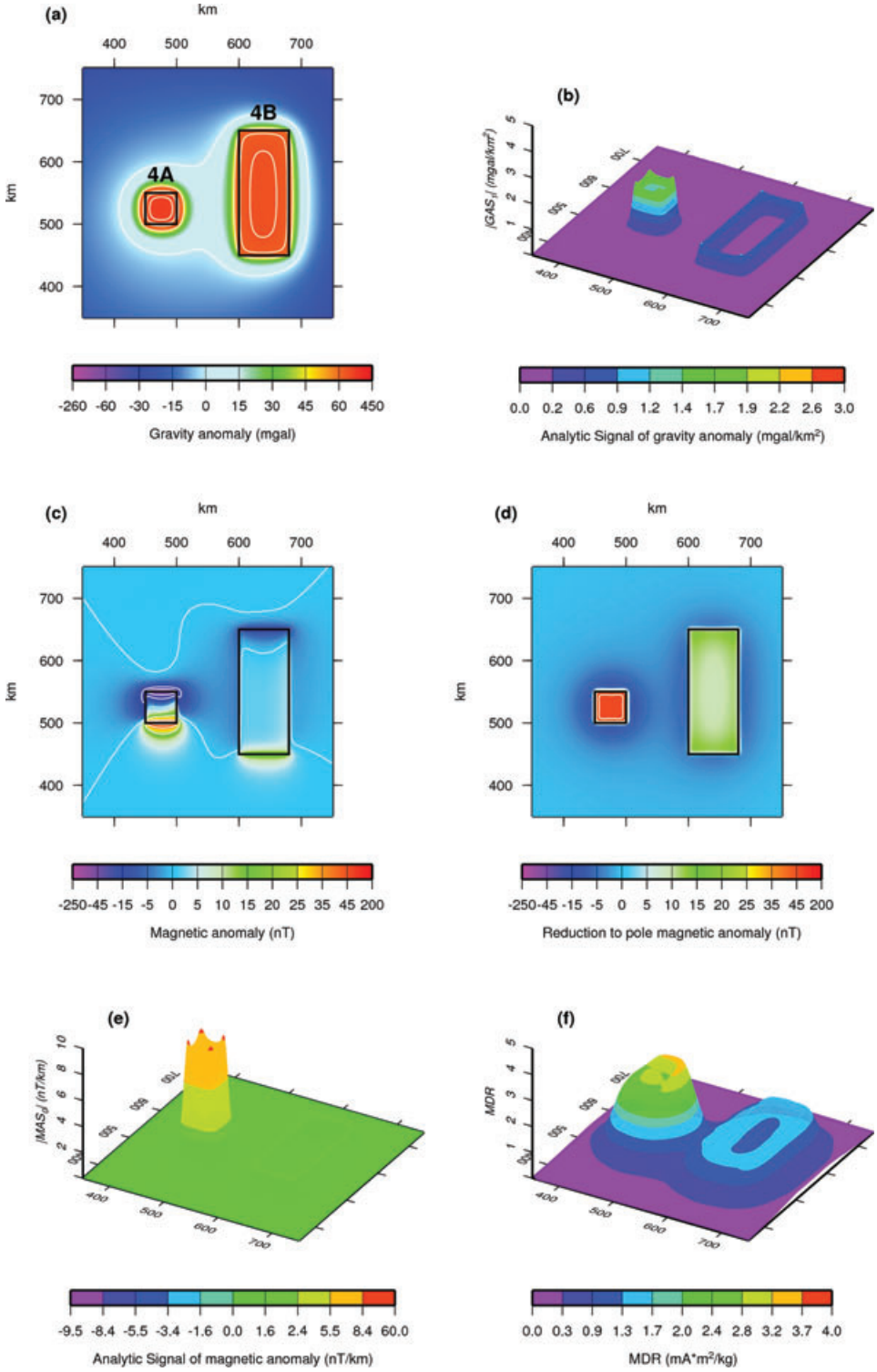

Figure 4. (a) Gravity anomaly, thick block indicate the source boundary, (b) amplitude of the gravity first-order analytic signal, (c) magnetic anomaly, thick block indicate the source boundary, (d) reduction to pole magnetic anomaly, (e) amplitude of the magnetic zero-order analytic signal and (f) MDR values distribution.

the MDR (Fig. 2f). In this 3-D test model, the MDR value contrast is 3.0 $mAm^2\ kg^{-1}$ between the background and source. In Fig. 2(f), we can see the maximum MDR values are distributed along the source boundary and the values are all near 3.0 $mAm^2\ kg^{-1}$. Therefore, in the simple source model, the proposed model can well identify the source boundary and its MDR value.

Then, we look at a model in which the horizontal size of the source is shorter than its depth. We construct a square prism of 2 km × 2 km × 10 km shown in Fig. 3. The distance to the top of the prism is 4 km. The density and magnetization contrast of the prism are 0.4 g cm^{-3} and 0.4 A m^{-1}. The following steps are the same as mentioned above. Then, the MDR result is shown in

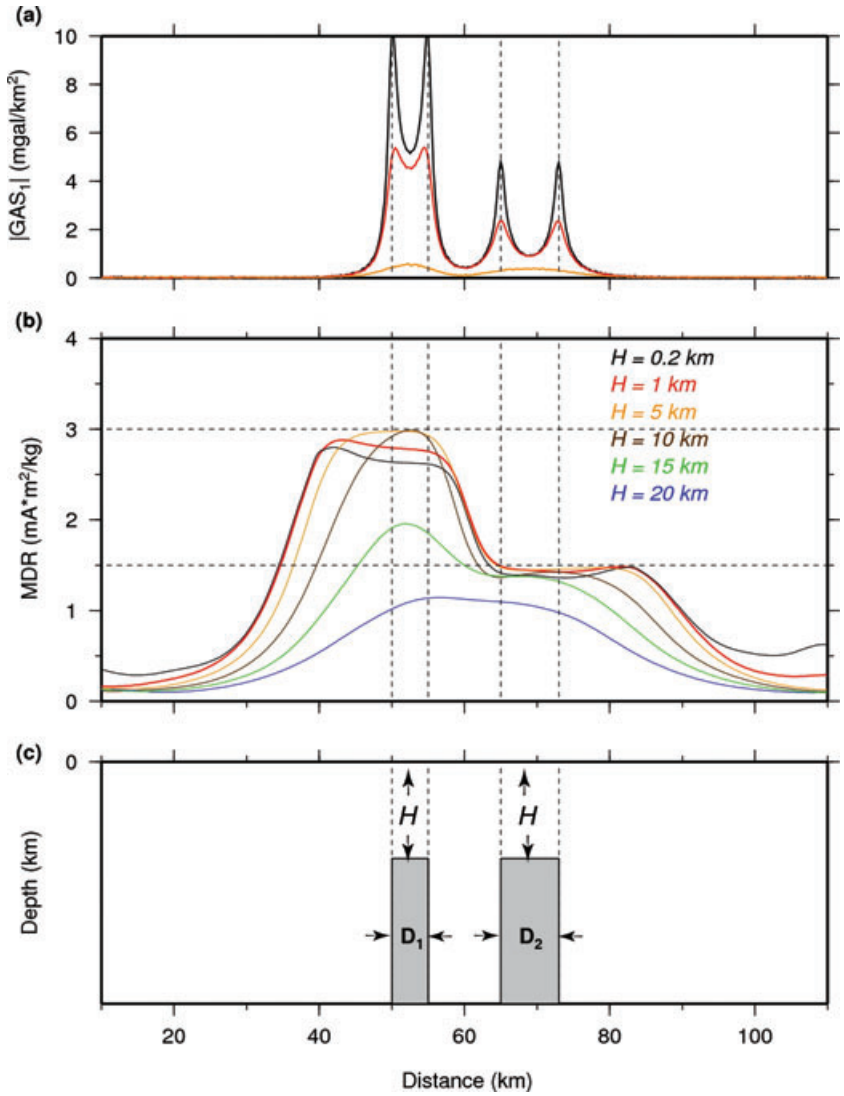

Figure 5. (a) Amplitude of the gravity first-order analytic signal, (b) MDR values distribution for different H (depth to the top surface of each prism) and (c) model geometry, H is variable, D_1 and D_2 indicate the width of prisms.

Fig. 3(f), the ratio equals to 0.92, it is not accurately revealed to 1.0. The error of calculated MDR value may be caused by interference from each side of the model. As the result, the maximum MDR value does not distribute in the border of the prism but focuses in the center. This result confirms with the assumption that near-surface structures can be characterized adequately by step models; deep structures can be characterized by dyke models.

In Fig. 4, we constructed two separate prisms: one is 50 km × 50 km × 20 km and the other is 200 km × 80 km × 20 km. The magnetization and density contrasts for the left prism are 1.2 A m^{-1} and 0.4 g cm^{-3}, and 0.3 A m^{-1}, 0.2 g cm^{-3} for the right prism, respectively. Other parameters are the same as model 1. The gravity anomaly is shown in Fig. 4(a) and the magnetic anomaly is shown in Fig. 4(c); the reduced to the pole magnetic anomaly is shown in Figs 4(d), (e) and (b) are the calculated amplitude of the analytic signal of the magnetic anomaly and gravity anomaly, respectively. On the basis of the analytic signals, we can calculate their MDR value, and the result is shown in Fig. 4(f). Theoretically, the MDR values are equal to 3.0 and 1.5 for left and right prisms. However, the MDR results do not accurately show to 3.0 and 1.5 for left and right prisms. The error of calculated MDR value may be caused by the mutual interference of the two sources. Although complex subsurface sources would influence the MDR value estimation, the maximum MDR values are still cluster around the source boundaries. In our case, the MDR values are approximately 90 per cent accurate compared to the theoretical value (Fig. 4f).

For cases 3 and 4, although the 3-D enhanced analytic signal method can avoid dependence on the ambient magnetic field (Hsu *et al.* 1996), magnetic sources interference may still affect the MDR estimation. We construct a model to illustrate this problem. The model shown in Fig. 5 includes two prisms: one is 5 km × 5 km × 5 km and the other is 20 km × 8 km × 5 km (Fig. 5c). The magnetic parameters are the same as in case 4 and H (depth to the top surface of each prism) is in a range from 1 to 20 km. We select a horizontal line cross the centre of these two prisms at y-axis 57.5 km, the estimated MDR results are given in Fig. 5(b) and the MDR value at the edge of each prism versus H/D_1 and H/D_2 (D_1 and D_2 indicate the width of prisms) are shown in Figs 6(a) and (b). In this test, we can see that the MDR estimation becomes worse when H/D value is larger (Figs 6a and b). The analytic signal method can help

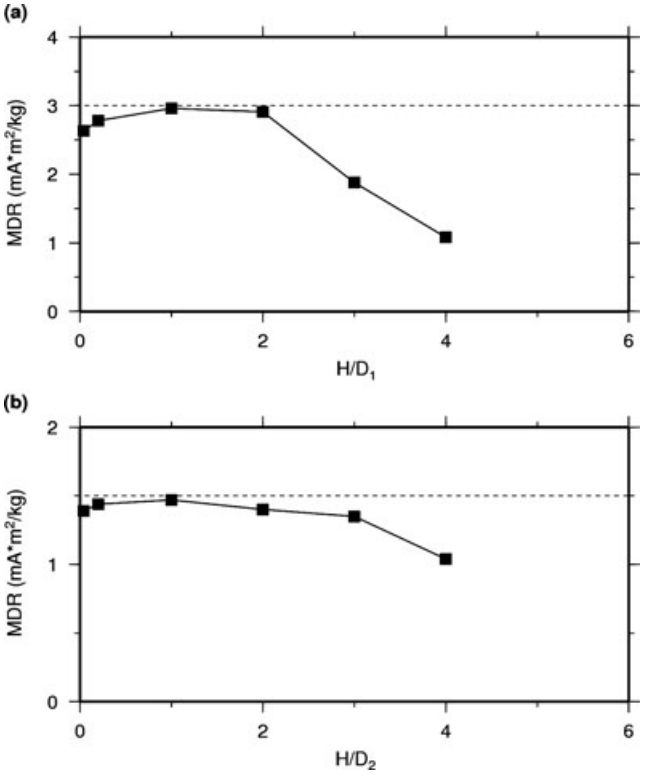

Figure 6. (a) MDR value at the edges of prism in terms of H/D_1 and (b) MDR value at the edges of prism in terms of H/D_2.

us to define the sources boundaries. However, as H increases, two nearby peak values of the analytic signal amplitude would merge to one maximum (Fig. 5a). Thus, the proposed method may not discriminate sources boundaries, and the MDR values also become uncertainty (Fig. 6).

4 DENSITY AND MAGNETIZATION OF GENERAL ROCKS

To have a better knowledge of MDR in real data, we compare the densities and susceptibilities of general rocks and minerals reported by Hunt *et al.* (1995). Based on the different composition materials, we can roughly separate these rocks into five types: (I) igneous rocks, (II) sedimentary rocks, (III) metamorphic rocks, (IV) non-iron-bearing minerals and (V) iron-bearing minerals (Table 2). Densities and susceptibilities of rocks do not have a clear proportion relation (Fig. 7a). According to the density and susceptibility of each rock, we can obtain the mass susceptibility (density/susceptibility) of each rock (Fig. 7b). It may reflect the characteristics of each type. This value is helpful in geophysical interpretation. In Fig. 7(b), mass susceptibility distribution can also been used to separate different kind of rocks. Here we estimate the relative MDR values instead of the absolute MDR (mass susceptibility) values. In Fig. 7(c), we use for example the clay as a reference, then the calculated MDR values of other material are relative to the clay.

In any given area where some knowledge of the magnetic properties of the rocks is available, the quantity MDR may suggest the most probable rock causing the anomaly. Even if we do not have any information about the densities or the magnetic properties of the rocks; knowledge of MDR alone also could provide information that can help us to speculate the rocks types roughly (Fig. 7c).

5 APPLICATION TO REAL DATA

To demonstrate the feasibility of the proposed method, we analyse gravity and magnetic data in the offshore of northern Taiwan.

5.1 Offshore northern Taiwan

The tectonics of offshore northern Taiwan has been dominated by a rifting system from late Cretaceous to Pleistocene, as opposed to the extensive folding and thrusting on the island during late Miocene to Pleistocene (Huang *et al*. 1992). Relic basin near the Mainland China Massif was first generated by a backarc rifting and subsequent convection induced by subduction and finally terminated by the subsequent collision of oceanic plate or the formation of volcanic arcs. The tectonic units are composed of basins and ridges (Huang *et al*. 1992). These ridges are probably composed of acid volcanic rocks of the Cretaceous that are overlain by late Palaeocene volcanic rocks (Sun 1982). The tectonic and basinal framework of offshore northern Taiwan is related to the evolution of relic backarc basin.

5.2 Magnetic and gravity data processing

The data shown in Figs 8(c) and (b) are extracted from the gravity and magnetic data sets of Hsu *et al.* (1998a), and the data sample interval equals to 1 km for MDR calculation. In the magnetic anomaly map, there are patterns of dipole magnetic fields in areas A and B. In this area, there are some volcanic intrusions or extrusions, such as Pengchiagu and Mienhuayu (Hsu *et al.* 1998a, Fig. 8a). In gravity anomaly map, the presence of area B is marked by an abrupt change in the FAA (Fig. 8c).

Based on the model IGRF10, the geomagnetic field inclination and declination offshore northern Taiwan are 37.80° and −3.56°, respectively. The magnetic reduction to pole data is shown in Fig. 8(d), and Pengchiagu, Mienhuayu and Huapinghsu are located in the relatively high magnetic anomaly area. Following the same procedure used for the test cases, the distribution of amplitudes of the zeroth-order magnetic and the first-order gravity analytic signal were obtained (1 min grid spacing). The amplitudes of the analytic signals of the gravity anomaly and magnetic anomaly are shown in Figs 8(e) and (f), respectively. The MDR value distribution is obtained (Fig. 9).

In Fig. 9, we can see the high MDR value concentrates on A, B and along northwestern coast of Taiwan. The MDR distribution pattern is similar to the reduction to pole magnetic anomaly pattern, except for some small areas. This may indicate the high MDR values are mainly resulted from high susceptibility materials. As mentioned above, Pengchiagu and Mienhuayu volcanic islands are located in area A (Hsu *et al.* 1998a), this geological feature is consistent with our calculation results.

5.3 Seismic data processing

Generally seismic reflection data can give us some information about the geometry of structures in the subsurface. In our MDR results, we can see the high MDR values concentrate on area A

Table 2. Density and susceptibility of rocks and minerals (Hunt *et al.* 1995).

Type	Density, ρ (g/cm^{-1})	Susceptibilities, κ (10^{-6} SI)	Mass susceptibility, κ/ρ (10^{-8} m^3 kg^{-1})
I. Igneous rocks			
Rhyolite	2.52	250–38 000	10–10 000
Andesite	2.61	170 000	6500
Granite	2.64	0–50 000	0–1900
Porphyry	2.74	250–210 000	9.2–7700
Diorite	2.85	630–130 000	22–4400
Diabase	2.91	1000–160 000	35–5600
Basalt	2.99	250–180 000	8.4–6100
Gabbro	3.03	1000–90 000	26–3000
Peridotite	3.15	96 000–200 000	3000–6200
Pyroxenite	3.17	130 000	4200
Igneous rocks	2.69	2700–270 000	100–10 000
Average acidic igneous rocks	2.61	38–82 000	1.4–3100
Average basic igneous rocks	2.79	550–120 000	20–4400
II. Sedimentary rocks			
Clay	1.70	170–250	10–15
Coal	1.35	25	1.9
Shale	2.10	63–18 600	3–886
Limestone	2.11	2–25 000	0.1–1200
Red sediments	2.24	10–100	0.5–5
Sandstones	2.24	0–20 900	0–931
Dolomite	2.30	−10 to 940	−1 to 41
Average sedimentary rocks	2.19	0–50 000	0–2000
III. Metamorphic rocks			
Quartzite	2.60	4400	170
Granulite	2.63	3000–30 000	100–1000
Schist	2.64	26–3000	1–110
Phyllite	2.74	1600	60
Serpentine	2.78	3100–18 000	110–630
Slate	2.79	0–38 000	0–1400
Gneiss	2.80	0–25 000	0–900
Amphibolite	2.96	750	25
Average metamorphic rocks	2.76	0–73 000	0–2600
IV. Non-iron-bearing minerals			
Ice	0.92	−9	−1
Graphite	2.16	−80 to −200	−3.7 to −9.3
Halite	2.17	−10 to −16	−0.48 to −0.75
Gypsum	2.34	−13 to −29	−0.5 to −1.3
Serpentinite	2.55	3100–75 000	120–2900
Orthoclase	2.57	−13 to −17	−0.49 to −0.67
Quartz	2.65	−13 to −17	−0.5 to −0.6
Calcite	2.83	−7.5 to −39	−0.3 to −1.4
Anhydrite	2.98	−14 to −60	−0.5 to −2.0
Forsterite	3.20	−12	−0.39
Magnesite	3.21	−15	−0.48
Celestite	3.96	−16 to −18	−0.40 to −0.45
Sphalerite	4.00	−31 to −750	−0.77 to −19
V. Iron-bearing minerals			
Montmorillonite	2.50	330–350	13–14
Illite	2.75	410	15
Biotites	3.00	1500–2900	52–98
Orthopyroxenes	3.59	1500–1800	43–50
Garnets	3.90	2700	69
Siderite	3.96	1300–11 000	32–270
Orthoferrosilite	4.00	3700	92
Olivine	4.32	1600	36
Fayalite	4.39	5500	130
Chromite	4.80	3000–120 000	63–2500
Jacobsite	4.99	25 000	500
Franklinites	5.21	450 000	8700

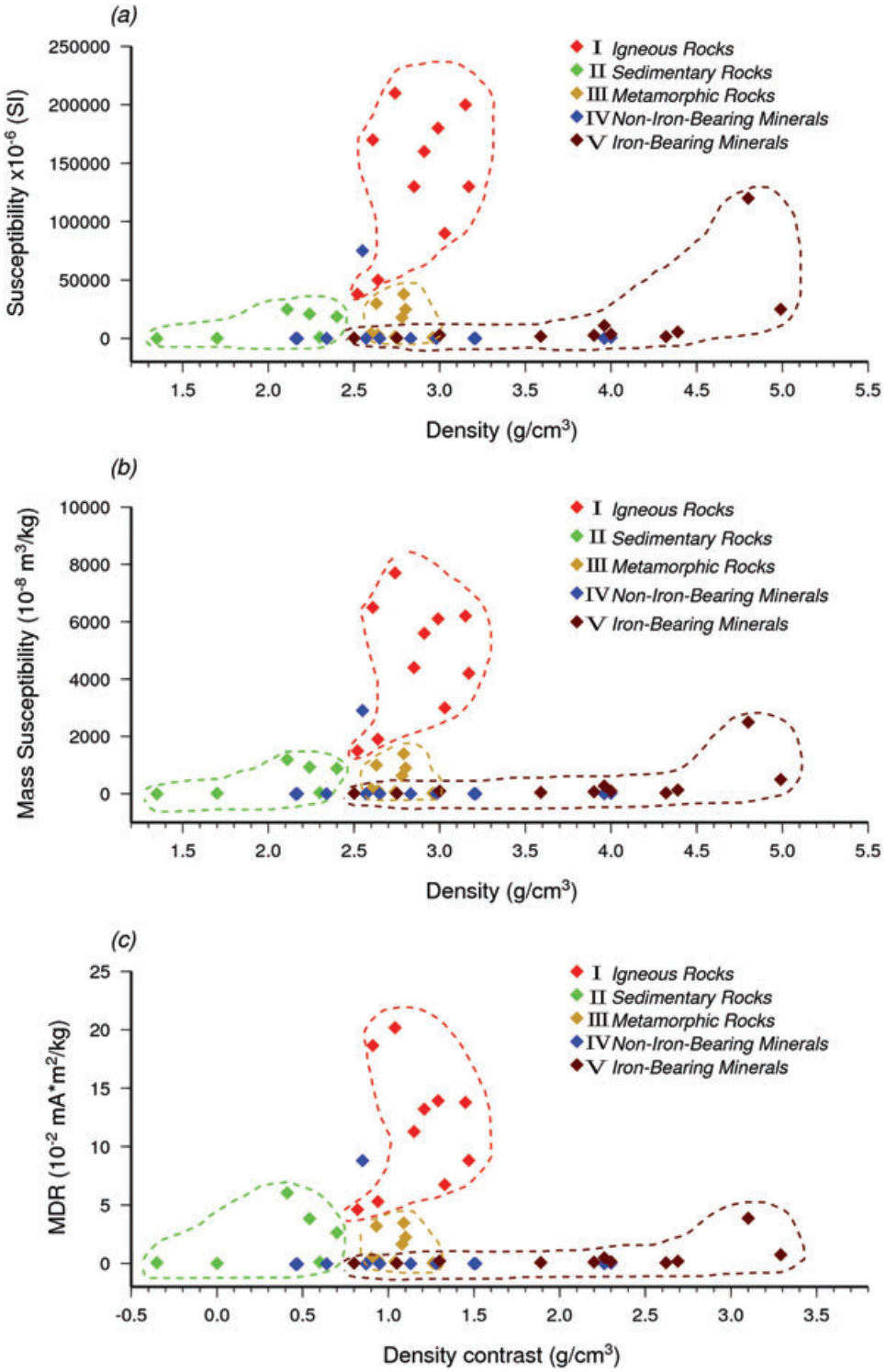

Figure 7. (a) Density dependence of susceptibility of selected rocks and minerals, (b) mass susceptibility of rocks and minerals distribution and (c) MDR value of rocks and minerals distribution.

(Fig. 9). To further investigate area A, we have analysed one multichannel seismic profile across area A (Fig. 9) to compare the results. We used the R/V Ocean Research Π to conduct one reflection seismic survey (cruise OR2–1146) across area A. The seismic profile shown in Fig. 10(b) was conducted with 12 channels reflection seismic experiment. The total GI gun source volume of 90 c.i. (45c.i. + 45c.i.) was used. The profile was conducted at a ship speed of 4.8 knots, a shot interval of 10 s (about 25 m), a sampling rate of 0.5 s and a record length of 3 s. We applied a 16–32-64–128 Hz bandpass filter and water velocity (1480 m s^{-1}) for stacking.

In Fig. 10(b), in the south side of seismic profile we can observe some clear reflection layers gradually deepening towards the north

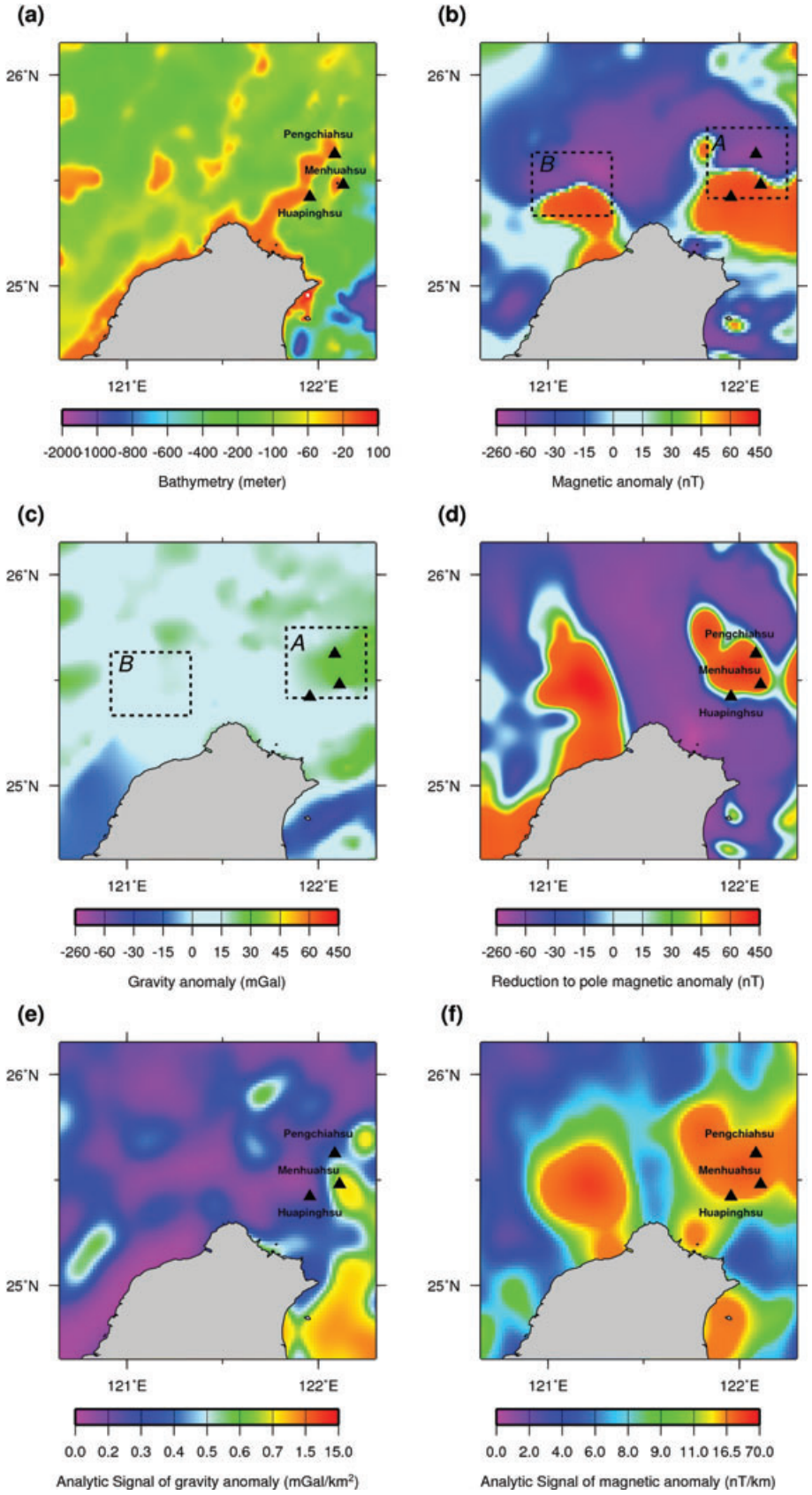

Figure 8. (a) Bathymetry map in offshore northern Taiwan, (b) magnetic anomaly map, (c) gravity anomaly map, (d) reduction to pole magnetic anomaly, (e) amplitude of the magnetic zero-order analytic signal and (f) amplitude of the gravity first-order analytic signal.

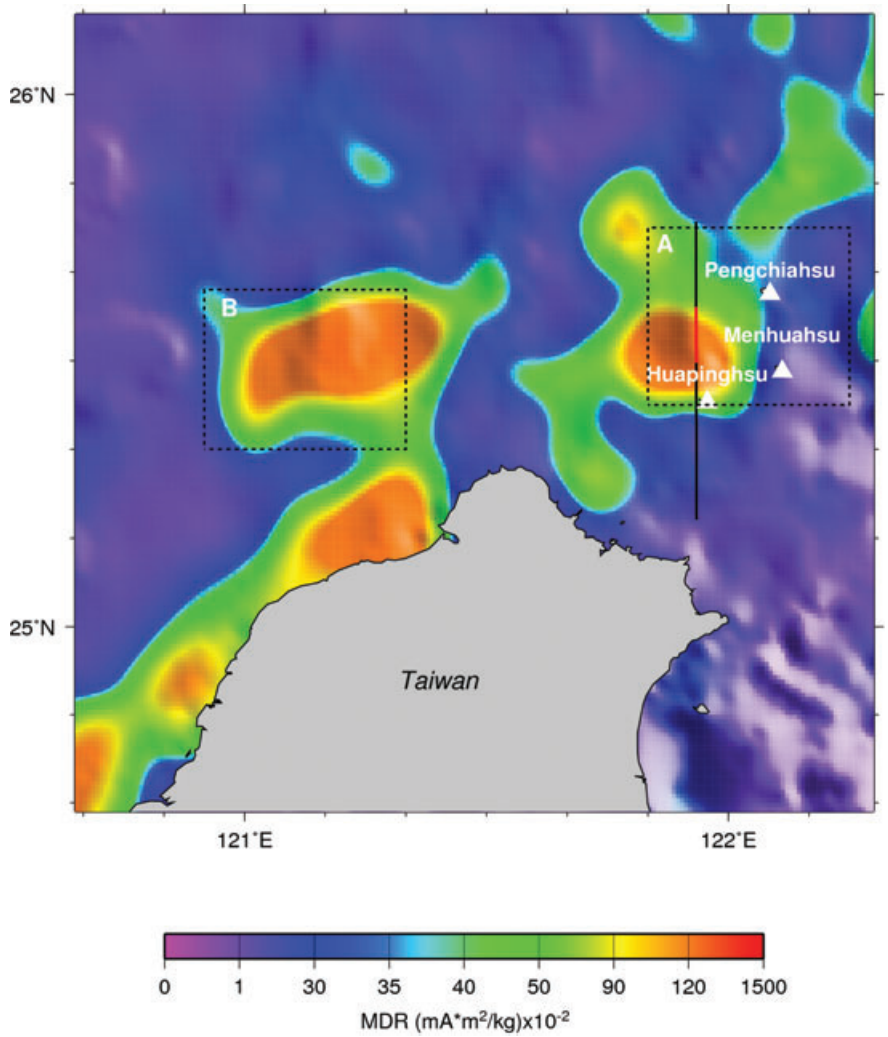

Figure 9. Magnetization/density ratio (MDR) values distribution; the heavy line indicates the multichannel seismic profile; the red line indicates the predicted source location; the white triangle indicates island positions.

yet mingled with some erosion phenomenon. However in the north part of Fig. 10(b), there is no obvious layers and cannot trace the basement. Therefore, we suggest that the compositions of materials in these two sides are different. The truncation of seismic sequences (Fig. 10b) has implied some uplift volcanic materials and caused seismic blanking. According to Hsu *et al.* (1998a), Pengchiagu and Mienhuayu are volcanic extrusions.

As the test in the 2-D model (Fig. 1), the maximum MDR value in Fig. 10(c) suggests a geological boundary. However, from seismic profile, there were no obvious layers observed in further north of Huapingshu. Consequently, only used seismic data (Fig. 10b) can't provide us enough information about a tectonic structure beneath this area. Hence, we use Hsu's method (Hsu 2002) to obtain structural boundary locations and structural indexes (Figs 10d and e). Because from magnetic data the structural index of the Euler method (Hsu 2002) is roughly equal to 1 (Fig. 10d), a dyke structure beneath this area (about 9 km) is suggested (Fig. 10e). The location of the converged solution in Fig. 10(e) is close to the distance where the maximum MDR value exists. Furthermore, we used the method proposed by Hsu *et al.* (1998b) to calculate the width of the dyke, $w = \sqrt{\frac{2d}{c_1} - d^2}$, where $c_1 = |\frac{A_1(0)}{A_0(0)}|$, d indicates the source depth; w indicates half-width of the dyke; $|A_0|$ and $|A_1|$ indicate the zeroth- and first-order analytic signal of magnetic data, respectively. We obtain the dyke width of 11.86 km. This result shows that the proposed method is helpful in geological interpretation. Moreover, high MDR value indicates that the material beneath the study area could be igneous rocks (type I in Fig. 7c).

6 CONCLUSION

On the basis of gravity and magnetic anomaly data, we have proposed a method by applying analytic signals to Poisson theorem to calculate the MDRs of geological structures. The advantage of using this method is that not only we can estimate the MDR distribution of the subsurface sources, we can also determine the geological boundary. The synthetic models and real data have shown that the proposed method is feasible, we find a dyke of igneous rocks in the Huapinghsu area offshore north Taiwan whose top surface is at 9.0 km beneath the sea surface and the dyke width is 11.86 km.

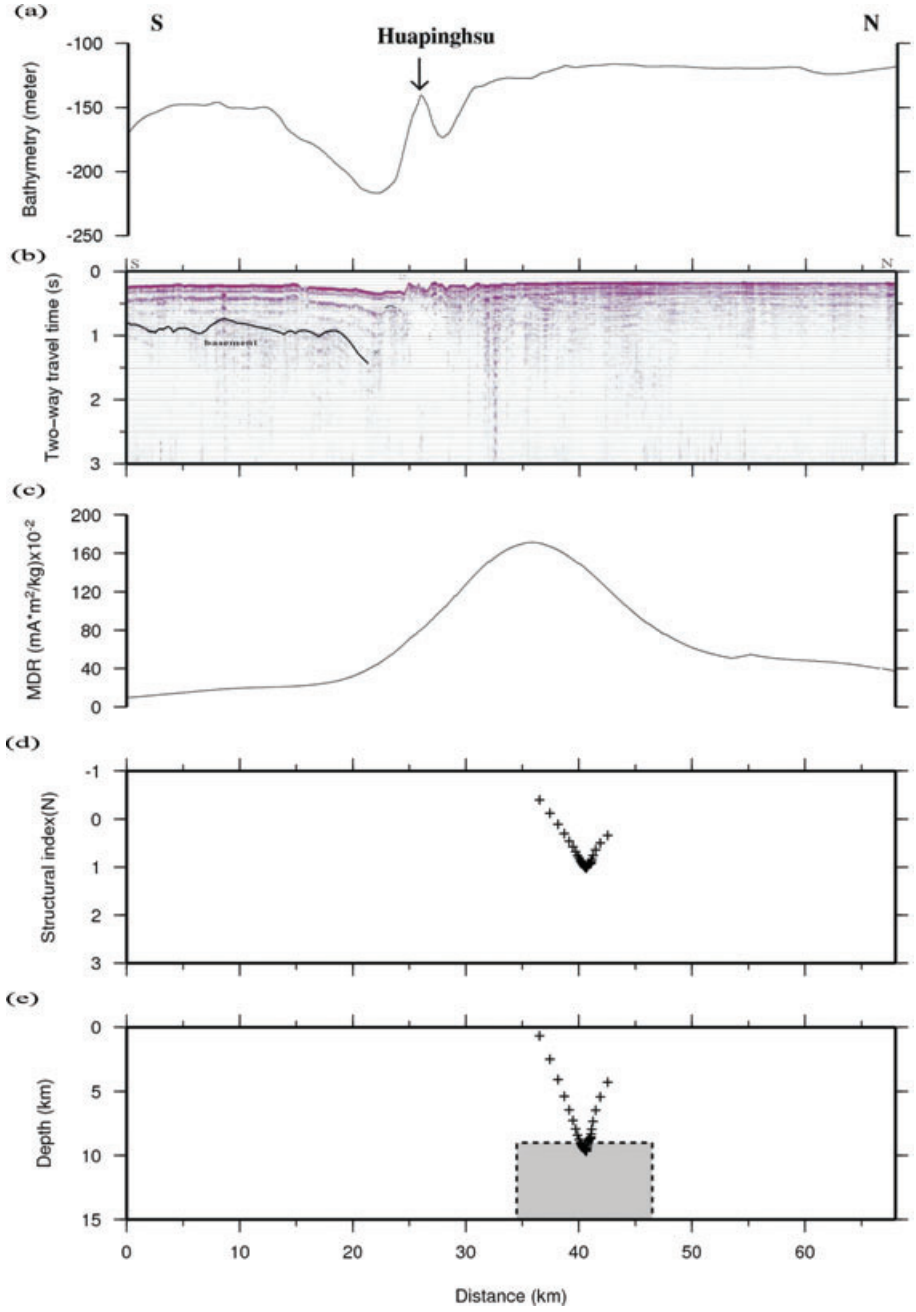

Figure 10. (a) The bathymetry data along the seismic profile, (b) seismic profile and its interpretation. Box T exists seismic blacking phenomenon. (c) MDR values; (d) structural index solutions; (e) depth solutions, shaded area indicate the dyke geometry.

ACKNOWLEDGMENTS

We are grateful to Prof C.-S. Lee for helping us collect reflection seismic profile. The comments and suggestions from editor Prof Michel Diament and two anonymous reviewers are appreciated. This study was under the grants of Central Geological Survey and National Science Council of Taiwan.

REFERENCES

Chandler, V.W. & Malek, K.C., 1991. Moving-window Poisson analysis of gravity and magnetic data from the Penokean orogen, east-central Minnesota, *Geophysics,* **56,** 123–132.

Chandler, V.W., Koski, J.S., Hinze, W.J. & Braille, L.W., 1981. Analysis of multisource gravity and magnetic anomaly data sets by moving-window application of Poisson theorem, *Geophysics,* **46,** 30–39.

Cordell, L. & Taylor, P.T., 1971. Investigation of magnetization and density of a North American seamount using Poisson's theorem, *Geophysics,* **36,** 919–937.

Garland, G.D., 1951. Combined analysis of gravity and magnetic anomalies, *Geophysics,* **16,** 51–62.

Grant, F.S. & West, G.F., 1965. *Interpretation Theory in Applied Geophysics,* McGraw-Hill, New York, NY.

Hildebrand, T.G., 1985. Magnetic terranes in the central United States determined from the interpretation of digital data, in *The Utility of Gravity and Anomaly Maps,* pp. 248–266, ed. Hinze, W.J., Soc. Exploration Geophysics, Tulsa, OK.

Hsu, S.K., 2002. Imaging magnetic sources using Euler's equation, *Geophys. Prospect.,* **50,** 15–25.

Hsu, S.K., Sibuet, J.-C. & Shyu, C.T., 1996. High-resolution detection of geologic boundaries from potential-field anomalies: an enhanced analytic signal technique, *Geophysics,* **61,** 373–386.

Hsu, S.K., Liu, C.S., Shyu, C.T., Liu, S.Y., Sibuet, J.-C., Lallemand, S., Wang, C.S. & Reed, D., 1998a. New gravity and magnetic anomaly maps un the Taiwan-Luzon region and their preliminary interpretation, *TAO,* **9,** 509–532.

Hsu, S.K., Coppens, D. & Shyu, C.T., 1998b. Depth to magnetic source using the generalized analytic signal technique, *Geophysics,* **63,** 1947–1957.

Huang, S.T., Ting, H.H., Chen, R.C., Chi, E.-R., Hu, C.C. & Shen, H.C., 1992. Basinal framework and tectonic evolution of offshore northern Taiwan, *Petrol. Geol. Taiwan,* **27,** 47–72.

Hunt, C.P., Moskowitz, B.M. & Banerjee, S.K., 1995. Magnetic properties of rocks and minerals, in *Rock Physics and Phase Relations: A Handbook of Physical Constants*, pp. 189–204, Am. geophys. Union, Washington, DC.

Mendonca, C.A., 2004. Automatic determination of the magnetization-density ratio and magnetization inclination from the joint interpretation of 2D gravity and magnetic anomalies, *Geophysics,* **69,** 938–948.

Poisson, S.D., 1826. Mémoire sur la théorie du magnétisme, Mémoires de I'Académie Royale des Sciences de I'Institut de Rrance, 247–348.

Roest, W.R., Verhoef, J. & Pilkington, M., 1992. Magnetic interpretation using the 3D analytic signal, *Geophysics,* **57,** 116–125.

Ross, H.P. & Lavin, P.M., 1966. In situ determination of the remnant magnetic vector of two-dimensional tabular bodies, *Geophysics,* **31,** 949–962.

Sun, S.C., 1982. The Tertiary basin of offshore Taiwan, in *Proceedings of the Second ASCOPE Conference and Exhibition,* pp. 125–135.

Wilson, G.D.V., 1970. The use of the Poisson relationship for separating the anomalies due to neighboring bodies, and for recongnizing inhomogeneities and structural deformation, *Bull. de Geofig. Teor. ed. Apl.,* **12,** 158–182.